Evolution of stress in individual grains and twins in a magnesium alloy aggregate

C. C. Aydıner,[1,*] J. V. Bernier,[2] B. Clausen,[3] U. Lienert,[4] C. N. Tomé,[1] and D. W. Brown[1]
[1]*Materials Science & Technology Division, Los Alamos National Laboratory, Los Alamos, New Mexico 87545, USA*
[2]*Engineering Technologies Division, Lawrence Livermore National Laboratory, Livermore, California 94551, USA*
[3]*Los Alamos Neutron Science Center, Los Alamos National Laboratory, Los Alamos, New Mexico 87545, USA*
[4]*Advanced Photon Source, Argonne National Laboratory, Argonne, Illinois 60439, USA*
(Received 12 November 2008; revised manuscript received 4 May 2009; published 21 July 2009)

This is an *in situ* measurement of the full stress tensor and its evolution in a growing deformation twin and, simultaneously, in the grain where the twin forms. The combined information provides a detailed picture of the grain-twin interaction. The three-dimensional x-ray diffraction method using 80.7 keV synchrotron x rays allows us to *in situ* investigate a grain within the bulk of a magnesium alloy (AZ31) sample that is compressed to activate the $\{10\bar{1}2\}\langle\bar{1}011\rangle$ tensile twin system. We observe that the stress state of the twin is drastically different from the one of the grain in which it is embedded. We analyze such result in terms of the shear transformation associated with twinning and the dimensional constraints imposed by the surrounding aggregate.

DOI: 10.1103/PhysRevB.80.024113 PACS number(s): 62.20.F−, 61.05.C−

I. INTRODUCTION

Crystallographic twinning is a strain accommodation mechanism extensively observed in hexagonal-close-packed (HCP) metals and, in general, in low-symmetry crystals.[1–3] Twinning transformations are induced by stresses acting along directions where dislocation glide is unfavorable: They are accompanied by crystallographic reorientation of grain domains, and localized shear. The nucleation and growth of such domains with increasing strain are at the basis of the hardening rate, texture evolution, and internal stress evolution observed when testing HCP[4–6] and low-symmetry aggregates. In particular, the cyclic deformation of magnesium and magnesium alloys exhibits dramatic Bauschinger effects and highly distorted hysteresis loops.[7,8] Clearly, advances in constitutive description and improved plastic formability of HCP metals will require a basic characterization of twinning mechanisms.

Recent elasto-plastic self-consistent (EPSC) polycrystal simulations of magnesium alloy AZ31, complemented with neutron-diffraction experiments, highlight the need for a more fundamental understanding and experimental characterization of twinning.[9,10] The reason is, in part, that while twin nucleation and growth take place inside individual grains, neutron diffraction, on the other hand, yields statistically averaged internal strains in the grains and the twin domains. Thus, although neutron diffraction provides excellent statistical insight, it offers limited information on the specific characteristic of the parent-twin-neighborhood interaction. Clearly, observations on the individual parent-twin interaction at the inherent length scale of the phenomenon would not only contribute to improve our understanding of twinning but also to the development of more accurate twin models and predictive capabilities.

Consequently, here, we use the emerging technique of three-dimensional x-ray diffraction (3DXRD)[11–14] to *in situ* monitor the twin nucleation and growth in individual grains inside the bulk of a polycrystalline aggregate. For this measurement $\{10\bar{1}2\}\langle\bar{1}011\rangle$ tensile twinning is activated in magnesium alloy AZ31. The main attributes of this study are the grain length scale of the measurement and the accomplishment of *tensorial* internal strain measurements. While there have been recent studies reporting evolution of specific *strain* components and volume fraction in the martensitic transformation of austenitic steels using the 3DXRD technique,[15,16] this is an *in situ* measurement of the evolving *full strain and stress tensors* in both parent grain and its twin as the latter nucleates and grows. Measuring the full stress tensor in the parent (or its twin) allows for resolving the stress on any plane, such as the $\{10\bar{1}2\}$ twin plane itself, which will be shown to yield critical insight. In addition, the evolution with applied stress of the twin volume fraction is derived directly from the 3DXRD data, which provides us with a quantitative measure of twin growth. The triaxial stress evolution of the parent and the twin is interpreted here in the light of the constraints placed on the parent and the twin by the surrounding polycrystalline medium.

II. EXPERIMENTAL

A. Procedure

Commercial magnesium alloy AZ31 has a nominal composition of 3 wt.% Al and 1 wt.% Zn, with restrictions on the transition metal impurities Fe, Ni, and Cu in order to improve the corrosion resistance. The alloy was obtained as a 1 in. (25.4 mm) thick hot-rolled plate in the soft annealed condition (O temper) with average grain size of 50 μm. The rolling texture of the plate has basal poles predominantly oriented perpendicular to the rolling plane.[4,5] Cylindrical compression samples of 1.2 mm diameter and 1.8 mm length are cut by electric discharge machining such that the cylinder axis coincides with the transverse direction of the plate. In this way, the texture of the sample favors grains with the *c* axis perpendicular to the compression direction, which provides a large fraction of grains favorably oriented to nucleate twins. Finally, the grains are grown to ~100 μm with a 1 h heat treatment at 500 °C.

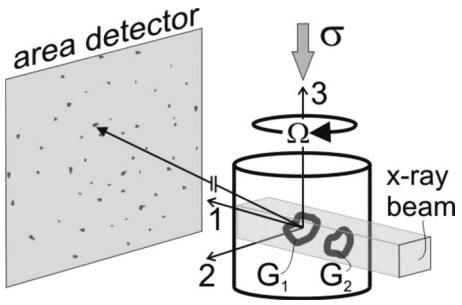

FIG. 1. Schematic of the experimental geometry. The cylindrical compression sample and the associated sample coordinate system.[1–3] The load is applied along axis 3. The area detector (40 $\times$40 cm^2) is 1.8m away from the sample. Targeted grain (G_1) is centered with respect to the Ω rotation axis as well as the 0.2 $\times$0.2 mm x-ray beam that engulfs it. The diffraction spots of G_1 appear on different images that are recorded on the area detector, each corresponding to one-degree Ω sweeps. Also shown is an arbitrary grain (G_2) in the path of the beam that also contributes spots to the images.

The *in situ* 3DXRD experiments were conducted at the 1-ID beamline of the Advanced Photon Source, Argonne National Laboratory. The layout of the experiment is illustrated in Fig. 1. Compressive loading was applied in displacement control with a purpose-built load fixture and measurements were performed at 20MPa increments. The sample was gradually compressed until the target stress is achieved and held at constant cross-head position for 3DXRD data acquisition. Since grains were intentionally grown to limit the number of diffraction spots, the 200$\times$200 μm^2 beam size gives a "spotty" diffraction pattern on the area detector. The 3DXRD technique relies on rotations (Ω) about the loading axis and high-energy (80.7 keV) monochromatic x rays. The sample is rotated about the loading axis, Ω, over a 120° range; single diffraction images are recorded while sweeping Ω at 1° intervals. This "Ω run" collects Bragg reflections (diffraction spots) from 20 to 25 crystallographic planes for each fully bathed diffracting grain. Here, the area detector, 1.79 m away from the sample, encompassed spots from hexagonal crystal plane families $\{10\bar{1}0\}$, $\{0002\}$, $\{10\bar{1}1\}$, $\{10\bar{1}2\}$, $\{11\bar{2}0\}$, $\{10\bar{1}3\}$, $\{20\bar{2}0\}$, $\{11\bar{2}2\}$, and $\{20\bar{2}1\}$. These frames were analyzed by the program GRAINDEX[5] that identifies all spots in the image stack and forms a database. Then, the program searches for crystallite orientations that would produce these spots.[11–13] From the list of orientations output by the program, four grains were selected for monitoring, based on (i) spot completeness, i.e., all (about 50) spots predicted for the grain are identified and (ii) their orientation. Three of the selected four grains were in the "twinning orientation," with their *c* axis lying roughly normal to the compression direction (axis 3). The fourth grain was chosen as a plastically soft orientation:[9] with its *c* axis making a 45° angle with the compression axis, soft basal slip is expected to dominate its plastic behavior. Once that the orientation of the parent is determined, one can calculate *unequivocally* where the diffraction spots of each twin variant should appear in the Ω images, and look for them. The appearance of diffraction spots at the predicted locations indicates that a particular variant has been activated.

The technique is costly in terms of experiment time since a separate Ω run is conducted for each grain at every load. Indeed, conducting Ω runs for four grains (120$\times$4=480 frames) at each load was only possible with the utilization of a state-of-the-art, high-speed area detector (GE Revolution 41RT, 41$\times$41 cm^2 area, 200$\times$200 μm^2 pixel size). We ensure that each target grain (depicted as G_1 in Fig. 1) is fully engulfed by the beam for the corresponding Ω-run range. Physically, this is achieved by bringing the target grain's volumetric center to the diffractometer center before its Ω run. As a result, the diffraction spots of a grain *in its corresponding* Ω run are all sampled from the entire volume of the grain. Obviously, this is necessary for unambiguous determination of both volume fraction and strain, described in the next section.

B. Data analysis

Prior to the analysis of the diffraction spots, all images were processed with background subtraction and corrected for the spatial distortion and the tilt of the area detector. Both corrections were characterized with NIST powder standard CeO_2. For this, a thin layer CeO_2 was positioned at the location of the sample (after the removal of the Mg sample) and the recorded diffraction image analyzed with the FIT2D[17] program. Recall that crystallographic planes contribute unambiguous spots in the Ω run for each target grain (the exact number depends on the grain's orientation). Two facts regarding the spots are worth noting. First, with few exceptions, each of the diffracting planes meets the diffraction condition twice, at slightly different Ω values. The corresponding pair of spots (the Friedel pair) is designated with Miller indices $(hk.l)$ and $(-h-k.-l)$. Second, each (hk.l) spot appears, in general, in more than one consecutive image. This means that the Ω breadth of a spot was, in general, more than 1°.

To analyze the data, a computer code was written in python™ to identify the spots automatically. Precisely, the spot identification consists of finding the consecutive images, *j*, that contain the spot, and, in each image *j*, detecting the pixels, *i*, that belong to the spot. The code features visualization tools to check the authenticity of the spots that have been picked by the automatic algorithm. This is necessitated by overlaps, namely, the other grains in the path of the beam (e.g., G_2 in Fig. 1) producing spots in the proximity of the target grain's spot. Inclusion of a foreign or compromised spot in the strain analysis proved to be very detrimental for strain accuracy. Such spots are discarded and every spot included in the analysis has been visually verified.

The first stage of analysis for an admitted diffraction spot is to determine its intensity and radius as measured from the beam center on the area detector. On each image *j*, the effective radius R_e^j and intensity I^j is given by $R_e^j=\Sigma_i R_i^j I_i^j$ and $I^j=\Sigma_i I_i^j$, respectively, where I_i^j and R_i^j are the intensity and the radius of the pixel *i*. Then, the effective radius of the spot, designated by R_e, is determined as the intensity-weighted average of R_e^j over *j* spots $R_e=\Sigma_j R_e^j I^j$. Further, the (total) intensity of a spot follows as $I=\Sigma_j I^j$.

For the measurement of the volume fraction of the twin (or parent) at a certain applied stress, the intensity of their

spots are compared to those of the parent grain prior to twinning. This comparison follows proper normalization that aims to remove all factors from the spot intensity apart from the size of the diffracting volume. Three such factors are accounted for here. The first is the normalization with respect to the incident beam intensity, which is measured in an ion chamber for each recorded image. The second is the structure factor normalization that also includes the effect of atomic scattering factors (e.g., Ref. 18, p. 122). The third is a geometric factor (Ref. 8, p. 36) specific to the 3DXRD technique. Depending on the choice of the compared spots, there is spread in the volume fraction computation. The standard deviation of this spread yields the error bar.

The first step in computing the lattice strain in the $(hk.l)$ plane is converting the measured radius (R_e) of the spots $(hk.l)$ and $(-h-k.-l)$ to d spacing with the Bragg's law.[18] After discarding the compromised spots, 10–20 such Friedel pairs are left. (The exact number, M, depends on the crystallite as well as the applied stress.) The $(hk.l)$ and $(-h-k.-l)$ spots that belong to the same plane are diametrically opposed on the $\{hk.l\}$ diffraction ring. Hence, when determining the d spacing of the crystal plane as an average of the Friedel pair, $d_{HK.L}=(d_{hk.l}+d_{-h-k.-l})/2$, the error in detector center is virtually eliminated. This greatly enhances the accuracy of the elastic strain given by

$$\varepsilon_{HK.L}=\frac{d_{HK.L}-d^0_{HK.L}}{d^0_{HK.L}}, \tag{1}$$

where

$$d^0_{HK.L}(a_0,c_0)=\left[\frac{4}{3}\frac{(h^2+hk+k^2)}{a_0^2}+\frac{1}{3}\frac{l^2}{c_0^2}\right]^{-1/2},$$

where a_0 and c_0 are the strain-free lattice parameters of the HCP crystal. The lattice strain is related to the elastic strain tensor, $\underline{\underline{\varepsilon}}$, through

$$\varepsilon_{HK.L}=\underline{n}_{HK.L}\cdot\underline{\underline{\varepsilon}}\cdot\underline{n}_{HK.L}, \tag{2}$$

where $\underline{n}_{HK.L}$ is the normal of the $(hk.l)$ plane. The equations for all M measured planes $(M>10)$ are put in the matrix form

$$\{\varepsilon_{\text{meas}}\}\approx[N]\cdot\{E\}, \tag{3}$$

where $\{\varepsilon_{\text{meas}}\}$ is the M-component vector of measured strains, each given by Eq. (1), $\{E\}$ is the six-component vector of the elastic strain tensor in Voigt notation, and $[N]$ is the $M\times 6$ plane-normal matrix. Then, the components of the elastic strain tensor in the crystal coordinates are given by least squares optimization (Penrose inverse) as

$$\{E\}=([N]^T[N])^{-1}[N]^T\{\varepsilon_{\text{meas}}\}. \tag{4}$$

Expressing the residual vector of the fit as $\{r\}=\{\varepsilon_{\text{meas}}\}-[N]\cdot\{E\}$, the normalized residual, e, is a normalized form of the residual vector modulus, given by

$$e=\sqrt{\frac{1}{M-6}\sum_{i=1}^{M}(r_i)^2}, \tag{5}$$

where M-6 is the degree of freedom in the fit. The error propagated to individual components of the strain tensor is given by $\delta E_i=\sqrt{\{[(N)^T(N)]^{-1}\}_{ii}}\cdot e$, $i=1,\ldots,6$.

The elastic strain tensor given by Eq. (4) is consistent with the position and spread of the diffraction spots, as discussed in Sec. B above. As a consequence, the strain tensor truly represents an average value over the spatial domain that contributes to the diffraction spots. The strain is likely to be uniform in the domain of the twin, especially in the initial stages of twinning, when the twin is a thin lamella that can be assimilated to an Eshelby inclusion. In the case of the parent, the strain field is likely to be rather homogeneous before twinning, while becoming increasingly distorted in the vicinity of the twin. As a consequence, the strain given by Eq. (4) for the parent will represent an average value. The same conclusions apply to the average stress tensor in a crystallite, $\underline{\underline{\sigma}}$, which is calculated from the *elastic* strain tensor using the generalized Hooke's law and the Mg single crystal stiffness.[19] The single crystal stiffness tensor of magnesium alloys vary less than 2% with alloying elements at concentrations below 5%.[20] Thus, in Voigt notation, the stress components are given by $\sigma_i=\Sigma_j C_{ij}E_j$ where C_{ij} is the stiffness tensor components and the error propagated to stress components can be evaluated as $(\delta\sigma_i)^2=\Sigma_j(C_{ij}\delta E_j)^2$.

It is worth noticing that here we report relative stresses, as is usually done in neutron diffraction work.[4–9] Relative stresses are referred to the initially unloaded sample. The absolute stress state is the sum of residual and relative stresses. The reason for using relative stresses is that they exclude any systematic error introduced in evaluating (a_0,c_0). Instead, this error affects the residual stresses. Hence, the results that will be reported here are not affected by the accuracy of the reference lattice parameters. For completeness, we note the nominal lattice parameter values used are $a_0=3.21745$ Å and $c_0=5.22176$ Å at detector distance $D=1788.9$ mm. In addition, considering that the sample was annealed, and that residual stresses of thermal origin are unlikely in Mg because the single crystal is thermally nearly isotropic, we expect relatively low values of intra and intergranular residual stresses in our sample.

III. RESULTS AND DISCUSSION

As load increases and more plasticity is introduced, the spread of the diffraction spots recorded at the detector increases (see "streak" in Fig. 3) as a result of increasing intragranular misorientation (mosaicity). As a consequence, the number of spots that need to be excluded from the analysis because of overlaps increases with load. Of the three grains that were selected and measured here, because they were favorably oriented for twinning, only one accumulated appreciable twinning before the spot-overlap problem precluded an accurate stress analysis (at an applied stress of about 90 MPa).

Figure 2 shows the orientation of the unit cell of this grain, and we will constrain our attention to it in what fol-

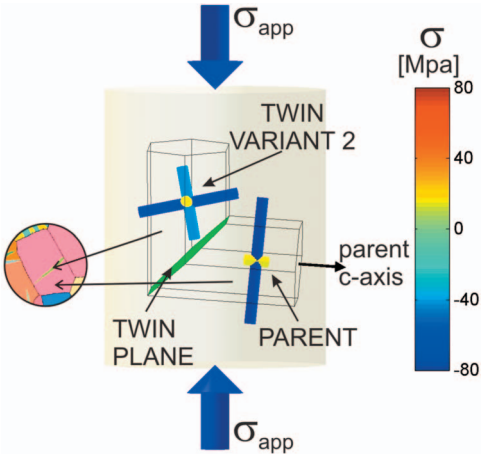

FIG. 2. (Color) Orientation of the hexagonal unit cells of the parent grain and the twin variant 2 in the bulk of the sample. The orientation of the common twin plane (green) is also shown. Triads depicting the principal axes of stress and the principal stress components are shown for the parent and variant 2 for an applied stress (σ_{app}) of 40 MPa. The length of the arm is proportional to the stress magnitude in that direction. In addition, each arm is color coded for stress values. In the inset on the left, the typical lamellar morphology of the twin is shown in an orientation imaging microscopy (OIM) micrograph of another AZ31 grain with equivalent twin/parent orientation.

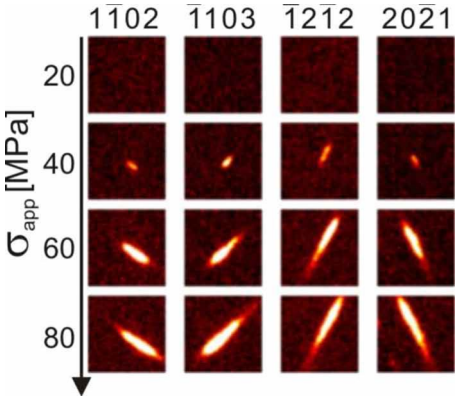

FIG. 3. (Color online) Predicted regions of interest (ROI) for selected (hkil) spots of twin variant 2. Each column shows the ROI of an (hkil) spot (at the Ω frame that the spot intensity is maximum) as a function of applied load. The appearance of the spot at the originally empty ROI (at 40 MPa) shows the nucleation of the twin, and the spot intensity increasing with load reflects the growth of the variant.

lows. The six variants in the $\{10\bar{1}2\}\langle\bar{1}011\rangle$ twin system are arbitrarily numbered 1–6 in this work, clockwise around the c axis of the hexagonal unit cell. In this grain, of approximate dimensions $140\times80\times150$ μm^3, the twin variants 2 and 5 have the higher resolved shear stresses, and are the ones that nucleate and grow with deformation. Figure 2 shows the orientation of variant 2, whose c axis is reoriented 86.6° with respect to that of the parent. This angle is characteristic of the $\{10\bar{1}2\}\langle\bar{1}011\rangle$ twin system in magnesium, and the shear strain associated with this transformation

$$\Delta\gamma_t = [(c/a)/\sqrt{3} - \sqrt{3}/(c/a)](\Delta V'/V), \tag{6}$$

leads to an extension along the c axis of the parent. In the grain presented here, the c axis lies nearly perpendicular to the vertical loading direction (see Fig. 2). Hence, compression induces a deviatoric tensile stress component along the c axis of the grain. Since magnesium lacks an easy dislocation mechanism to allow elongation along the c axis,[2] the twin variants 2 and 5 are activated, and the grain expands laterally in the horizontal (1–2) plane. The c axis of variant 5 (not shown in Fig. 2) deviates a mere 6.8° from that of variant 2.

Once that the orientation of the parent is determined, one can calculate unequivocally where the diffraction spots of each twin variant should appear in the Ω runs. The appearance of diffraction spots at the predicted locations indicates that a particular variant has been activated. An independent confirmation that the twin is contained in the parent grain is that the sum of their calculated volume fractions remains constant through loading. Accordingly, the first two rows of Fig. 3 depict the emergence of the variant 2 at 40 MPa external compression. As strain increases, the volume fraction of the twin variant increases, and so does the intensity of the diffraction spots (rows 3 and 4 in Fig. 3). Quantitatively, all spots associated with each individual variant should yield the same volume fraction (following proper normalization). In addition, the latter should be consistent with the evolving volume fraction of the parent grain. At each load, we verify the conservation of the total crystal volume. The volume fraction of the parent and the twins as well as the mentioned verification is shown in Fig. 4. Here, at an applied stress of 40 MPa, both twin variants are captured shortly after their emergence, each with volume fraction of about 0.6% of the parent grain. At 80 MPa, variants 2 and 5 have grown to 18 and 10% of the initial parent volume, respectively. Note that the analysis is precluded beyond applied stresses of 100 MPa for the parent, 90 MPa for variant 2, and 80 MPa for variant 5. For each, too many Friedel pairs are invalidated by overlaps for meaningful analysis at these respective loads.

Before proceeding with the stress states of the twins and the parent, let us make two remarks: First, the typical normalized residual of the strain tensor fit [Eq. (5)] for both the

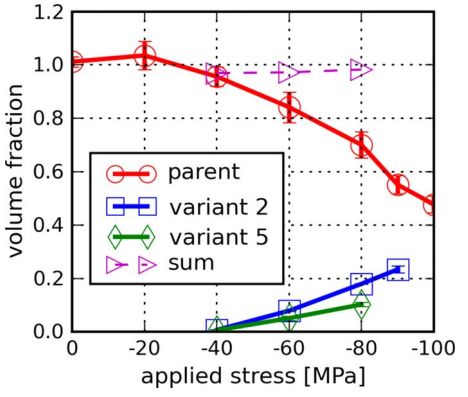

FIG. 4. (Color online) Volume fractions of the parent and the twin variants as a function of applied stress. The sum of all volume fractions is also shown for verification.

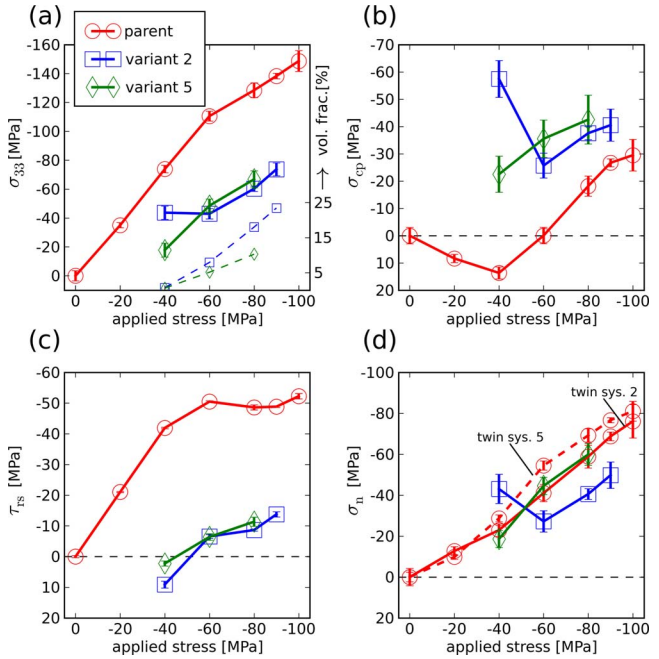

FIG. 5. (Color online) Projections of the stress tensors of the parent and twin variants along selected sample and crystal directions as a function of applied stress: (a) σ_{33}, crystal stress component along the compression axis (sample axis 3), and volume fractions of the twin variants (dashed lines). (b) σ_{cp}, the component of the stress tensor along the *c* axis of the *parent*. (c) τ_{rs}, the resolved shear stress on the twin plane along the twin direction. (d) σ_n, the stress projected along the twin plane normal of the respective variants.

parent and the twins ranged from 30×10^{-6} to 60×10^{-6} and the error propagated to the stress components was typically under 5MPa. To our knowledge, this level of precision in the strain tensor determination is unprecedented for the 3DXRD technique and is largely achieved through the utilization of visualization codes to avoid overlapping diffraction spots. Second, we note that the residual stresses are expected to be small due to the annealing procedure applied to the sample. Further, the *shear* stress components in the crystal reference system are independent of the reference lattice parameters, and for the grain of the study the maximum magnitude of the three shear components is 6 MPa. This serves to argue that the relative stresses calculated are close to the absolute stresses.

The stress state of the parent and the variant 2 twin is shown in Fig. 2, for an external applied stress of 40 MPa, in terms of the principal stress components and the directions of the eigenvectors. Because of the grain orientation, the principal axes of stress in grain and twin are close to the macroscopic ones. While Fig. 2 is meant to provide a 3D picture of the stress tensor at 40 MPa, Fig. 5 presents numerical values of specific stress components for parent and twin variants as a function of applied load. In Fig. 5(a) σ_{33} denotes the crystal stress component along the compression axis (sample axis 3). In Fig. 5(b), σ_{cp} is the component of the crystal stress tensor along the *c* axis of the *parent* (shown in Fig. 2). Figure 5(c) shows τ_{rs}, the resolved shear stress on the twin plane along the twin direction for both parent and twin grains. For clarity, only τ_{rs} for variant 2 in the parent is shown in Fig. 5(c), as the curve for variant 5 is virtually identical. It has to be kept in mind that the stress tensors for parent and twins represent an average over the corresponding crystal volume. However, when it is first observed the twin is a narrow lamella embedded in the parent and representing 0.6% of the parent's volume, and thus its stress can be assumed to be uniform and not to affect significantly the parent average. Figure 5(d) shows the stress in parent and twins projected along the twin plane normal, σ_n.

Note that when the applied stress is −40 MPa, σ_{33} in the parent is at a much higher level: −74 MPa [see Fig. 5(a)]. This indicates that this orientation is plastically "hard:" As a consequence, its deformation is mostly elastic and it carries more load than other grains at this stage of loading. (The monitored plastically soft grain carries −38 MPa at this stage.) The elastic behavior of the parent is further confirmed by the fact that its stress tensor components approximately double when the applied load goes from −20 to −40 MPa.

Twin nucleation and growth is a local process where the elastic strain in a region of the grain transforms into a localized irreversible shear. Once the energy barrier for transformation is exceeded the energy of the system decreases, and there is a tendency to "overshoot.[9]" If the parent was free to deform, a kink would form in it at the location of the twin domain. Such tendency, however, is counteracted by the constraint imposed by the surrounding grains, which induces a backstress which tends to prevent the parent to shear locally. The most obvious manifestation of such reaction is given by Fig. 5(c). Increasing τ_{rs} in the parent on the twin planes of variants 2 and 5 (the ones with higher resolved shear) eventually leads to their activation at about −40 MPa applied stress. At the initiation of twinning, the resolved shear τ_{rs} in the twin plane of variants 2 and 5 exhibits opposite sign than the average shear on the same plane in the grain. Further, notice that as the twin fraction increases, the parent's τ_{rs} tends to saturate. The natural assertion is that any tendency to increase τ_{rs} in the parent triggers the growth of the twin(s), which in turn relaxes τ_{rs}. Although the shears in the twins eventually adopt the same sign as in the parent, they remain much lower as the twins grow, indicating the sustained reaction from the surroundings to accommodate the localized twin shear. A more subtle conclusion emerges from the fact that τ_{rs} should be equal for the parent and the twin across the twin plane due to traction-continuity considerations. Yet, the τ_{rs} that is averaged from the entire parent volume [Fig. 5(c)] is distinctly higher, which points to high stress-gradients near the twin interfaces.

Figures 5(a) and 5(b) complement the analysis and provide further insight. At −40 MPa applied compression, the stresses in the twin domain are consistent with the shear back-stress discussed above, resolved along other directions. Figure 5(a) shows that, along the loading direction, the average σ_{33} in the parent is −74 MPa, much larger than σ_{33} in variant 2 (−43 MPa) or variant 5 (−20 MPa). As for the transverse stresses σ_{cp}, they show a large sign reversal inside the incipient twins [Fig. 5(b)]: while the stress is 13 MPa for the parent, it is −57 and −22 MPa in variants 2 and 5, respectively. This result is consistent with and confirms the statistical data of neutron diffraction.[9] As the twins grow to a

non-negligible fraction of the parent, they tend to affect more the average stress in the parent. Because the twin shear has an extension component along the *c* axis of the parent, it tries to expand the length of the parent along the *c* axis. However, the surrounding grains resist the expansion and, past −60 MPa applied stress, this reaction induces an increasingly compressive stress in the parent [see Fig. 5(b)].

The normal stress on the twin plane for the two variants within the parent grain, see Fig. 5(d), adopts values of approximately $\frac{1}{4}$ of the applied load in the elastic region, consistent with expressing an axial stress in a system rotated approximately 45°. The normal stress in the twins is systematically lower than the one calculated from the parent average and, since there has to be traction continuity at the twin interface, this result points at normal gradients within the parent near the twins. This difference provides further evidence of the localized reaction to the twin shear induced by the surrounding medium.

IV. SUMMARY

Here we report a sophisticated 3DXRD experimental technique, capable of tracking the full stress tensor in a grain and an evolving twin. In addition, this work also sheds light onto the coupling that takes place between a grain in the bulk and the surrounding neighbors when the twinning transformation takes place inside the grain. The current study features the following advances: (1) Stress evolution inside single grains in the bulk is studied while undergoing twinning. It is concluded that the surrounding polycrystalline medium plays a larger role in the stress development in the twin and the parent than recent neutron diffraction experiments lead us to believe;[9] (2) the twin in the targeted grain is monitored in relation to its parent, as opposed to an arbitrary twin in the bulk; (3) the unique capability to compute three-dimensional stress states gives access to essential stress components such as τ_{rs} at every stage of the twin evolution; (4) the analysis of spot intensities allows one to quantify the volume fraction of the evolving twins.

While here we study the deformation mechanism of twinning, which is relevant to the plastic response of Mg, its alloys, and other HCP systems, the same technique would be applicable to martensitic transformations in steels and shape memory alloys. In the future, we envisage that clusters of grains will be studied to further understand the interaction with neighbors. It is expected that a detailed mechanical description of twinning in HCPs will emerge from this work. This will, in turn, facilitate developing realistic polycrystal models that will resolve the complicated internal stresses brought about by twinning and provide predictive capability to the mechanical behavior of widely used HCP metals such as magnesium, titanium and zirconium.

ACKNOWLEDGMENTS

This work was supported by the Office of Basic Energy Science (DOE) through Project No. FWP 06SCPE401. The authors are indebted to A. Jain and S. R. Agnew of University of Virginia for their help in sample preparation. Use of the Advanced Photon Source was supported by the U.S. Department of Energy, Office of Science, Office of Basic Energy Sciences, under Contract No. DE-AC02-06CH11357.

*Present address: Mech. Eng. Dept., Bogazici University, Turkey; can.aydiner@boun.edu.tr

[1] J. W. Christian and S. Mahajan, Prog. Mater. Sci. **39**, 1 (1995).
[2] C. N. Tomé, S. R. Agnew, M. A. M. Bourke, W. R. Blumenthal, D. W. Brown, G. C. Kaschner, and P. Rangaswamy, Mater. Sci. Forum **408–412**, 263 (2002).
[3] M. H. Yoo and J. K. Lee, Philos. Mag. A **63**, 987 (1991).
[4] S. R. Agnew, D. W. Brown, and C. N. Tomé, Acta Mater. **54**, 4841 (2006).
[5] D. W. Brown, S. R. Agnew, M. A. M. Bourke, T. M. Holden, S. C. Vogel, and C. N. Tomé, Mater. Sci. Eng., A **399**, 1 (2005).
[6] F. Xu, R. A. Holt, and M. R. Daymond, Acta Mater. **56**, 3672 (2008).
[7] C. H. Caceres, T. Sumitomo, and M. Veidt, Acta Mater. **51**, 6211 (2003).
[8] L. Wu, A. Jain, D. W. Brown, G. M. Stoica, S. R. Agnew, B. Clausen, D. E. Fielden, and P. K. Liaw, Acta Mater. **56**, 688 (2008).
[9] B. Clausen, C. N. Tomé, D. W. Brown, and S. R. Agnew, Acta Mater. **56**, 2456 (2008).
[10] C. J. Neil, B. Clausen, S. R. Agnew, and C. N. Tomé (unpublished).
[11] E. M. Lauridsen, S. Schmidt, R. M. Suter, and H. F. Poulsen, J. Appl. Crystallogr. **34**, 744 (2001).
[12] R. V. Martins, L. Margulies, S. Schmidt, H. F. Poulsen, and T. Leffers, Mater. Sci. Eng., A **387–389**, 84 (2004).
[13] H. F. Poulsen, *Three-Dimensional X-ray Diffraction Microscopy: Mapping Polycrystals and their Dynamics* (Springer, Berlin, 2004).
[14] S. Schmidt, S. F. Nielsen, C. Gundlach, L. Margulies, X. Huang, and D. J. Jensen, Science **305**, 229 (2004).
[15] P. Hedström, U. Lienert, J. Almer, and M. Odén, Mater. Lett. **62**, 338 (2008).
[16] P. Hedström, J. Almer, U. Lienert, and M. Odén, Mater. Sci. Forum **524–525**, 821 (2006).
[17] A. P. Hammersley, ESRF Internal Report No. ESRF97HA02T, 1997 (unpublished).
[18] B. D. Cullity, *Elements of X-ray Diffraction* (Addison-Wesley, Reading, MA, 1956).
[19] G. Simmons and H. Wang, *Single Crystal Elastic Constants and Calculated Aggregate Properties: A Handbook* (MIT Press, Cambridge, MA, 1970).
[20] A. R. Wazzan and L. B. Robinson, Phys. Rev. **155**, 586 (1967).